Pressure effects on the electronic structure and superconductivity of $(TaNb)_{0.67}(HfZrTi)_{0.33}$ high entropy alloy

K. Jasiewicz,[1] B. Wiendlocha,[1,*] K. Górnicka,[2] K. Gofryk,[3] M. Gazda,[2] T. Klimczuk,[2] and J. Tobola[1]

[1]*Faculty of Physics and Applied Computer Science, AGH University of Science and Technology, Al. Mickiewicza 30, 30-059 Krakow, Poland*

[2]*Faculty of Applied Physics and Mathematics, Gdańsk University of Technology, ul. Narutowicza 11/12, 80-233 Gdańsk, Poland*

[3]*Idaho National Laboratory, Idaho Falls, Idaho 83415, USA*

(Received 5 August 2019; published 4 November 2019; corrected 5 June 2020)

Effects of pressure on the electronic structure, electron-phonon interaction, and superconductivity of the high entropy alloy $(TaNb)_{0.67}(HfZrTi)_{0.33}$ are studied in the pressure range 0–100 GPa. The electronic structure is calculated using the Korringa-Kohn-Rostoker method with the coherent potential approximation. Effects of pressure on the lattice dynamics are simulated using the Debye-Grüneisen model and the Grüneisen parameter at ambient conditions. In addition, the Debye temperature and Sommerfeld electronic heat capacity coefficient were experimentally determined. The electron-phonon coupling parameter λ is calculated using the McMillan-Hopfield parameters and computed within the rigid muffin-tin approximation. We find that the system undergoes the Lifshitz transition, as one of the bands crosses the Fermi level at elevated pressures. The electron-phonon coupling parameter λ decreases above 10 GPa. The calculated superconducting T_c increases up to 40–50 GPa and, later, is stabilized at the larger value than for the ambient conditions, in agreement with the experimental findings. Our results show that the experimentally observed evolution of T_c with pressure in $(TaNb)_{0.67}(HfZrTi)_{0.33}$ can be well explained by the classical electron-phonon mechanism.

DOI: 10.1103/PhysRevB.100.184503

I. INTRODUCTION

High-pressure studies of superconducting materials have brought about the latest breakthrough in the field of superconductivity. The record high T_c of 203 K in H_3S [1] and 250 K in LaH_{10} [2] at $P > 150$ GPa were recently reported, and theoretical predictions show that even larger values of T_c are possible [3,4]. As superconductivity in these materials is mediated by the electron-phonon interaction, recent discoveries also turned attention to the effect of extreme pressure on superconductivity in other materials, including bulk conventional superconductors. This includes recent high-pressure studies on superconductivity in Nb-Ti alloy [5] and $(TaNb)_{0.67}(HfZrTi)_{0.33}$ high entropy alloy (HEA) [6], on which we are focusing in this work.

High entropy alloys [7,8] contain five or more elements and, due to stabilization by the configurational entropy, form simple "monoatomic" crystal structures such as cubic bcc or fcc, with statistical occupation of the single-crystal site. The first superconducting HEA, $Ta_{34}Nb_{33}Hf_8Zr_{14}Ti_{11}$[9], was reported in 2014. It crystallizes in a *Im*-3*m* bcc type of structure, with a lattice parameter of 3.36 Å. In this system, all atoms randomly occupy (2a) crystal site (on average). It is a type-II superconductor with the transition temperature of $T_c = 7.3$ K. Experimental data as well as theoretical calculations [10] suggest conventional mechanism of superconductivity with a relatively strong electron phonon coupling parameter $\lambda \sim 1$. Several other examples of superconducting HEAs were later reported [11–13], however, the TaNbHfZrTi family is still the most investigated one [9,10,14,15]. When the atomic concentration is slightly changed to $Ta_{33.5}Nb_{33.5}Hf_{11}Zr_{11}Ti_{11}$ [15] [denoted as $(TaNb)_{0.67}(HfZrTi)_{0.33}$ or TNHZT in short], superconducting transition temperature slightly increases to 7.7 K. This alloy also hosts a cubic-body-centered crystal structure, with the lattice parameter of 3.34 Å.

When the external pressure is applied, T_c of $(TaNb)_{0.67}(HfZrTi)_{0.33}$ increases up to about 10 K at around 50–60 GPa and then it remains practically constant up to about 100 GPa. After that, it slightly decreases to 9 K at 190 GPa [6]. In our work we investigate effects of pressure on the electronic structure and superconductivity in this disordered system to better understand microscopic mechanisms controlling these interesting $T_c(P)$ characteristics. As the crystal structure was determined experimentally to about 96 GPa [6], we perform our studies in the pressure range from 0 to 100 GPa. The electronic structure is calculated using the Korringa-Kohn-Rostoker method with the coherent potential approximation (KKR-CPA) [16–19]. From the KKR-CPA results, by using the rigid muffin tin approximation (RMTA) [20], the McMillan-Hopfield parameters are calculated. Effect of pressure on the lattice dynamics is simulated using the Debye model and Grüneisen parameter γ_G. To obtain γ_G it becomes necessary to determine the volume thermal expansion coefficient, thus experimental measurements of the crystal structure evolution with temperature were performed. Additionally, to ensure the consistency of the analysis, the low-temperature heat capacity was measured on the same sample to obtain T_c, Debye temperature θ_D, and the Sommerfeld coefficient γ. As a final result, the pressure evolution of the electron-phonon coupling parameter $\lambda(P)$ and the superconducting critical temperature $T_c(P)$ are determined.

*wiendlocha@fis.agh.edu.pl

II. METHODOLOGY

A. Synthesis and x-ray crystallography

The $Ta_{0.335}Nb_{0.335}Hf_{0.11}Zr_{0.11}Ti_{0.11}$ sample was prepared by melting the required high-purity elements, i.e., tantalum foil (99.9%), niobium pieces (99.99%), hafnium pieces (99.99%), zirconium foil (99.8%), and titanium pieces (99.99%). The elemental metals were arc melted to a single metallic button under an argon atmosphere on a water-chilled copper plate. A piece of zirconium was used as a getter at each melting steps. After the initial melt, the sample nugget was turned and remelted three times to ensure the optimal mixing of the constituents. Mass loss during the synthesis was smaller than 1% and the resulting material was hard and silver in color.

The phase purity of the obtained material was checked by x-ray diffraction (XRD) using a Philips X'pert Pro MPD with Cu K_α radiation. The sample exhibited ductility, and therefore could not be ground. Because of that, for qualitative and quantitative characterization the sample had to be converted into a plate form. In order to prepare the sample for the XRD analysis, the button was cut into smaller piece and then transformed into a plate using hydraulic press. The mechanical handling did not cause any sample contamination. The plate was put on the Al_2O_3 (corundum) sample holder and mounted in a small furnace inside a diffractometer. Above 400 °C the sample oxidizes and, hence, the XRD analysis in higher temperatures was not continued. The lattice parameter for TNHZT at different temperatures was estimated from the LeBail fit using a HIGHSCORE program.

B. Heat capacity

Heat-capacity measurements were carried out using a Quantum Design Physical Property Measurement System (PPMS) Evercool-II. The two-τ relaxation method was used to measure the specific heat without external magnetic field and under 8 T magnetic field, in the temperature range 1.9–10 K. The sample was attached to the measuring stage by using Apiezon N grease to ensure good thermal contact.

C. Electronic structure

Electronic structure calculations were performed using the Korringa-Kohn-Rostoker method with the coherent potential approximation (KKR-CPA) [16–19] to account for atomic disorder. Crystal potential of the muffin-tin type was constructed using the local density approximation (LDA), Perdew-Wang parametrization [21], and in the semirelativistic approach. Angular momentum cutoff was set to $l_{\max} = 3$. Highly converged results were obtained for about 450 **k**-points grid in the irreducible part of Brillouin zone for self-consistent cycle and 2800 **k** points for the densities of states (DOS) computations. Muffin-tin radius was set to the largest nonoverlapping spheres (i.e., $R_{\mathrm{MT}} = a\sqrt{3}/4$) and the Fermi level ($E_F$) was accurately determined from the generalized Lloyd formula [17]. It is worth noting that the KKR-CPA method has already been successfully applied to study different physical properties of high entropy alloys [22–25].

Electron-phonon coupling and its evolution under external pressure is studied using the so-called rigid muffin-tin approximation (RMTA). This method has been successfully applied to many superconducting materials, mostly containing transition metal elements [20,26–31] and, more recently, to the HEA $Ta_{34}Nb_{33}Hf_8Zr_{14}Ti_{11}$ [10] at ambient pressure. In this approach, the electron-phonon interaction is decoupled into electronic and lattice contributions. The coupling parameter λ is computed as

$$\lambda = \sum_i \frac{\eta_i}{M_i \langle \omega_i^2 \rangle}, \tag{1}$$

where η_i are the McMillan-Hopfield parameters [32,33] computed for each of the atoms i in the unit cell, M_i is the atomic mass, and $\langle \omega_i^2 \rangle$ is the properly defined average square atomic vibration frequency (see the discussion of the frequency moments in the Supplemental Material [34]). Within RMTA, McMillan-Hopfield parameters are calculated using the band-structure related quantities [20,26,28] employing the expression

$$\eta_i = \sum_l \frac{(2l+2)\, n_l(E_F)\, n_{l+1}(E_F)}{(2l+1)(2l+3) N(E_F)} \left| \int_0^{R_{\mathrm{MT}}} r^2 R_l \frac{dV}{dr} R_{l+1} \right|^2, \tag{2}$$

where $V(r)$ is the self-consistent potential at site i, R_{MT} is the radius of the ith MT sphere, $R_l(r)$ is a regular solution of the radial Schrödinger equation (normalized to unity inside the MT sphere), $n_l(E_F)$ is the lth partial DOS per spin at the Fermi level E_F, and $N(E_F)$ is the total DOS per primitive cell and per spin. For a more detailed discussion of the approximations involved in this methodology, see, e.g., Refs. [28,29] and references therein.

In the case of a random alloy, where a single-crystal site i is occupied by several different atoms that have different concentrations, modification of Eq. (1) is necessary. In calculations of λ for binary alloys having similar atomic masses of elements (e.g., Nb-Mo), where one can expect similar denominators in Eq. (1), the McMillan-Hopfield parameters obtained from self-consistent KKR-CPA calculations, were simply weighted by atomic concentrations c_i [35], and were predicting composition dependence of λ reasonably well. Besides, in the case of a monoatomic system that has a Debye-type phonon spectrum, $\langle \omega_i^2 \rangle$ may be reasonably well approximated using the experimental Debye temperature [35–37] as $\langle \omega^2 \rangle = \frac{1}{2}\theta_D^2$ (see Supplemental Material [34] for the derivation of this formula). That is especially useful in the present case of a multicomponent HEA since it allows to estimate λ without knowledge of the phonon spectrum. As the Debye temperature represents the characteristic frequency of the whole system, we use it in combination with the concentration-weighted average atomic mass. In this approach, the denominator in Eq. (1) takes the form $M_i \langle \omega_i^2 \rangle \simeq \langle M \rangle \frac{1}{2}\theta_D^2$, where $\langle M \rangle = \sum_i c_i M_i$. The final formula for the electron-phonon coupling (EPC) parameter λ of HEA used in our work becomes

$$\lambda = \frac{\sum_i c_i \eta_i}{\frac{1}{2}\langle M \rangle \theta_D^2}, \tag{3}$$

where McMillan-Hopfield parameters η_i of each atom in the system are computed in the self-consistent KKR-CPA calculations and c_i is the atomic concentration of the element. As mentioned above, this approach was recently applied to the

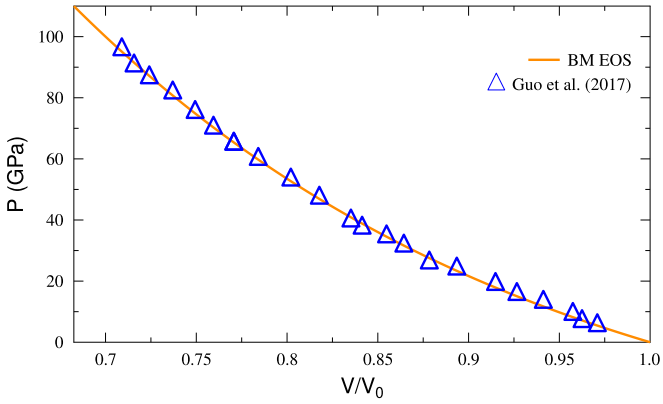

FIG. 1. Pressure dependence of the unit-cell volume. Points correspond to the experimental data [6] and line is determined from the fitted Birch-Murnaghan equation of state.

first superconducting high entropy alloy $Ta_{34}Nb_{33}Hf_8Zr_{14}Ti_{11}$ [10] at ambient pressure ($T_c = 7.3$ K). The value of $\lambda = 1.16$ was obtained in good agreement with the value of $\lambda = 0.98$ determined from the renormalization of the electronic heat-capacity coefficient γ. Here, the same approach is applied to $(TaNb)_{0.67}(HfZrTi)_{0.33}$ system to study evolution of superconducting properties under pressure.

As far as the crystal structure is concerned, high-pressure synchrotron x-ray diffraction measurements were performed in the pressure range from 0 to 96 GPa and it was shown that $(TaNb)_{0.67}(HfZrTi)_{0.33}$ maintains the bcc structure since no structural distortion was observed [6]. As there is no information on the crystal structure above this pressure, we limit our studies to the pressure range from 0 to 100 GPa. Available experimental data of volume vs pressure are shown in Fig. 1 and were fitted to the third-order Birch-Murnaghan equation of state [38]:

$$P(V) = \frac{3}{2}B\left[\left(\frac{V}{V_0}\right)^{-\frac{7}{3}} - \left(\frac{V}{V_0}\right)^{-\frac{5}{3}}\right] \times \left\{1 + \frac{3}{4}(B' - 4)\left[\left(\frac{V}{V_0}\right)^{-\frac{2}{3}} - 1\right]\right\}, \quad (4)$$

where V_0 is the equilibrium volume. Bulk modulus of $B = 177.35$ GPa and its derivative $B' = 2.87$ were obtained and are used in the subsequent analysis.

D. Evolution of Debye temperature with pressure

The Debye temperature of TNHZT θ_D^0 was measured only at ambient conditions [15], therefore, it was also necessary to simulate its pressure dependence to calculate $\lambda(P)$ and $T_c(P)$ using Eq. (3). This can be performed using the analytic model based on the Grüneisen parameter γ_G [40] where

$$\gamma_G(V) = -\frac{\partial \ln \theta_D}{\partial \ln V}. \quad (5)$$

As the volume compression (in our case) reaches 30% (see Fig. 1), a variation of the Grüneisen parameter with pressure (volume) has to be taken into account. This can be done using the so-called second-order Grüneisen parameter q:

$$q(V) = \frac{\partial \ln \gamma_G(V)}{\partial \ln V}, \quad (6)$$

which also may be pressure dependent. Equations (5) and (6) cannot be solved in a simple way as both γ_G and q are volume-dependent parameters. Assuming that the next logarithmic derivative is constant [41]

$$q'(V) = \frac{\partial \ln q(V)}{\partial \ln V} = \text{const}, \quad (7)$$

we may write $q(V)$ as a power-law relation

$$q(V) = q_0 \zeta^n, \quad (8)$$

where $\zeta = V/V_0$, n is a material-dependent constant parameter, and $q_0 = q(V_0)$ is the value at ambient conditions. Such approximation leads to the formula for $\gamma_G(V)$ [42]:

$$\gamma_G(V) = \gamma_G^0 e^{[\frac{q_0}{n}(\zeta^n - 1)]}. \quad (9)$$

Once $\gamma_G(V)$ is calculated the Debye temperature for a given volume (or equivalently pressure) is computed from

$$\theta_D(V) = \theta_D^0 \left(\frac{V}{V_0}\right)^{-\gamma_G(V)}. \quad (10)$$

Input parameters, required to compute $\theta_D(V)$, are ambient-pressure Debye temperature θ_D^0 and ambient-pressure Grüneisen parameter γ_G^0, which have not been determined for our system yet. To obtain γ_G^0 we have performed the volume thermal expansion coefficient α measurements, described in the next section. This allows to calculate the Grüneisen parameter at ambient conditions [40]

$$\gamma_G^0 = \frac{\alpha B V_0 N_A}{C_V}, \quad (11)$$

where V_0 is the primitive cell volume, N_A is the Avogadro number, and C_V is the molar constant-volume heat capacity taken as the Dulong-Petit limit of 24.94 ($\mathrm{J\,K^{-1}\,mol^{-1}}$). The second-order Grüneisen parameter is given by the following relation [43,44]:

$$q_0 = 1 + \delta_T - B', \quad (12)$$

where δ_T is the so-called Grüneisen-Anderson parameter [45]

$$\delta_T \equiv \frac{\partial \ln \alpha}{\partial \ln V}. \quad (13)$$

Using the work of Dugdale and MacDonald [46], Chang *et al.* obtained a simple relation between δ_T and γ_G^0 [47]:

$$\delta_T = 2\gamma_G^0. \quad (14)$$

Finally, second-order Grüneisen parameter may be calculated at ambient conditions as [47]

$$q_0 = 1 + 2\gamma_G^0 - B'. \quad (15)$$

Bulk modulus values B and B' were determined above from the $P(V)$ fit, thus, the only parameter which remained to be determined is the power-law coefficient n from Eq. (8). Unfortunately, there are no available literature data to estimate n, even for the constituent elements of TNHZT. To overcome this difficulty, first-principles phonon calculations in the pressure range of 0–100 GPa were performed for elemental Nb and

TABLE I. Computed and experimental values of the Debye temperature θ_D [32,48–50], the bulk modulus B, the pressure derivate of the bulk modulus B' [51], the Grüneisen parameter γ_G^0 [52], and the second-order Grüneisen parameter q_0 [Eq. (15)] at ambient conditions.

	θ_D (K)	B (GPa)	B'	γ_G^0	q_0
Nb (calc.)	271	163	3.52	1.55	0.14
Nb (expt.)	270–280	169	4.02	1.59	0.16
Ta (calc.)	219	194	3.787	1.427	0.067
Ta (expt.)	229–258	194	3.80	1.64	0.48

Ta, which are the main components of our HEA and have the same bcc crystal structure. This allowed us to validate the above-described method of calculating $\theta_D(P)$ as well as to obtain some information about the value of n.

Calculations of the phonon densities of states for Nb and Ta were performed using a QUANTUM ESPRESSO software [53,54]. We used projected augmented wave (PAW) pseudopotentials [55,56], with the Perdew-Burke-Ernzerhof generalized gradient approximation for the exchange-correlation potential [57]. First, phonon densities of states $F(\omega)$ were computed for various pressures and then the Debye temperature was calculated, based on the mth moment of the phonon spectrum:

$$\mu_m = \int_0^{\omega_{\max}} \omega^m F(\omega) d\omega \Big/ \int_0^{\omega_{\max}} F(\omega) d\omega, \tag{16}$$

$$\omega_D(m) = \left(\frac{m+3}{3}\mu_m\right)^{1/m}. \tag{17}$$

Among many available formulas for the "theoretical" Debye temperature (see Refs. [40,58] for more details) we choose the one, which corresponds to the correct representation of the heat capacity for $T > \theta_D$, i.e., $m = 2$, and $k_B\theta_D = \hbar\omega_D(2)$. However, since our materials have a simple acoustic phonon spectrum, θ_D computed using different values of m do not change in more than 5%. It should be noted that there is no conflict between Eqs. (16) and (17) and approximation $\langle\omega^2\rangle = \frac{1}{2}\theta_D^2$. To avoid any confusions, we explain the difference between $\langle\omega^2\rangle$ [that enters Eq. (1)] and the second moment of the phonon DOS function in the Supplemental Material [34].

Computed and experimental values of the bulk modulus B, its pressure derivative B', the Grüneisen parameter γ_G^0, and the second-order Grüneisen parameter q_0 for Nb and Ta are gathered in Table I. The second-order Grüneisen parameter q_0 is calculated using Eq. (15). The θ_D^0 parameter obtained from the phonon calculations and at zero pressure is 271 K for Nb and 219 K for Ta. The calculated Debye temperature of Nb remains in a very good agreement to the experimental values, which span the range of 270–280 K [32,48]. The θ_D^0 of Ta is slightly smaller than the literature values that range from 229 K [49] via 245 K [50], up to 258 K [32]. Grüneisen model calculations of $\theta(P)$ were performed using the computed θ_D^0 and other parameters, shown in Table I and for several values of n, ranging from 4 to 16. The values of $\theta(P)$, calculated directly from phonon DOS under pressure (shown in Supplemental Material [34]) and from the Grüneisen model for representative values of n, are compared

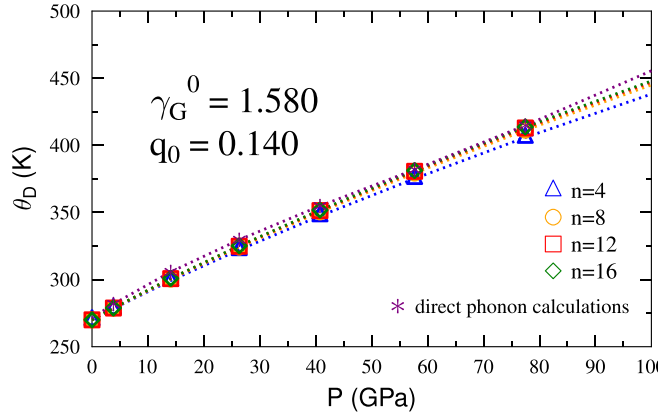

FIG. 2. Pressure dependence of θ_D of niobium from the direct phonon calculations and from the Grüneisen model for several values of n.

in Fig. 2 for Nb and Fig. 3 for Ta. In the case of Nb, an almost perfect agreement is found. Larger deviation is seen for Ta, but still the differences between the model and first-principles calculations are smaller than 10%. It is also worth noting that our model calculations of $\theta_D(P)$ for Ta remain in a very good agreement with the quasiharmonic approximation calculations of Liu *et al.* [39]. The general observation is that the pressure dependence of θ_D is quite well captured by the Debye-Grüneisen model, which contains only one free parameter n. Moreover, the computed $\theta_D(P)$ are not very sensitive to the particular choice of n due to relatively small q_0 values. In the case of Nb, where the agreement is better, $n = 16$ seems to be the best choice. Therefore, this value will be assumed in the analysis of HEA, where due to the presence of chemical disorder a phonon spectrum was not calculated.

To summarize the methodology section, electron-phonon coupling constant λ is calculated using Eq. (3), McMillan-Hopfield parameters are computed from band-structure results using Eq. (2), ambient-pressure values of the Debye temperature θ_D^0 and the Grüneisen parameters γ_G^0 and q_0 are taken from experiment, and the evolution of θ_D with pressure is modeled using Eqs. (9) and (10), where $n = 16$ is assumed.

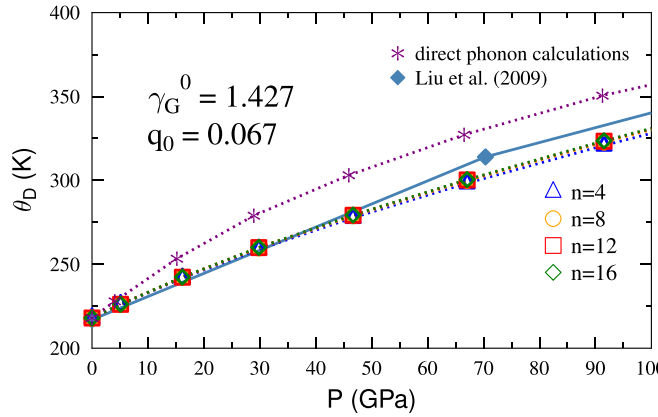

FIG. 3. Pressure dependence of θ_D of tantalum from the direct phonon calculations, from the Grüneisen model for several values of n, and from the quasiharmonic calculations of Liu *et al.* [39].

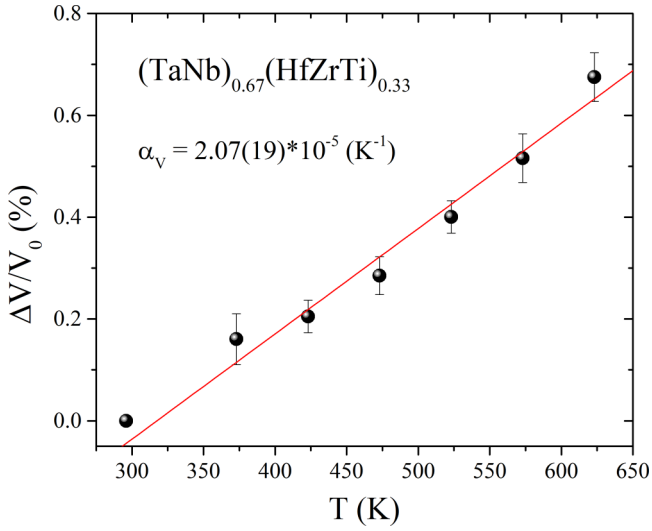

FIG. 4. Temperature dependence of a relative change of the unit-cell volume. The lattice parameter was obtained by the LeBail method. A cubic *Im*-3*m* (space group No. 229) structure was used as a starting model.

III. RESULTS AND DISCUSSION

A. Thermal expansion and heat capacity

The $(TaNb)_{0.67}(HfZrTi)_{0.33}$ as-cast sample was characterized using x-ray diffraction method (XRD). The measurement was first performed at room temperature and then at temperatures from 100 °C up to 400 °C with a step of 50°. The XRD pattern is shown in the Supplemental Material [34] and contains only sharp Al_2O_3 (holder) reflections and reflections that were indexed with an I-centered cubic phase. A cubic lattice parameter for TNHZT was refined using the LeBail method and HIGHSCORE software. A relative change of a unit-cell volume ($\Delta V/V_0$) vs temperature is presented in Fig. 4. The volumetric thermal expansion coefficient was found to be $\alpha = 2.07(19) \times 10^{-5}$ K^{-1} and is comparable to those obtained for the constituting metals [for which it changes from 17.1 (Zr) to 27 (Ti), given in (10^{-5} K^{-1})].

The temperature dependence of the electronic heat capacity C_{el}/T of $(TaNb)_{0.67}(HfZrTi)_{0.33}$ is presented in Fig. 5(a). The experimental data were collected under zero (open circles) and applied magnetic field (close circles). The C_{el} was obtained from the relation $C_p = C_{el} + C_{ph}$, where $C_{ph} = \beta T^3$ is the low-temperature ($T < \theta_D/50$) phonon contribution. In order to obtain β, the heat capacity in the normal state was measured and the data are presented in Fig. 5(b), plotted as C_p/T vs T^2. In the normal state C_p can be analyzed by $C_p = \gamma T + \beta T^3$, where γT is the contribution from the conduction electrons. The fit is represented by a solid red line with the fitting parameters $\gamma = 7.7(1)$ mJ mol^{-1} K^{-2} and $\beta = 0.193(2)$ mJ mol^{-1} K^{-4}. Then, we can calculate the Debye temperature from the relation $\theta_D = [(12\pi R)/(5\beta)]^{1/3}$, where R is the gas constant. Both the Sommerfeld parameter and Debye temperature $\theta_D = 216(1)$ K are in good agreement with those reported previously [15] ($\gamma = 7.97$ mJ mol^{-1} K^{-2}, $\theta_D = 225$ K). The sharp anomaly at $T_c = 7.6$ K, seen in the C_{el}/T, confirms a bulk nature of superconductivity in the studied sample. A normalized jump of the specific heat $\Delta C/\gamma T_c = 1.93$ is comparable to that reported in Ref. [15]. The estimated value exceeds the one expected for weak-coupling BCS superconductors $\Delta C/\gamma T_c = 1.43$, indicating that $(TaNb)_{0.67}(HfZrTi)_{0.33}$ is a an intermediate- or strong-coupling superconductor.

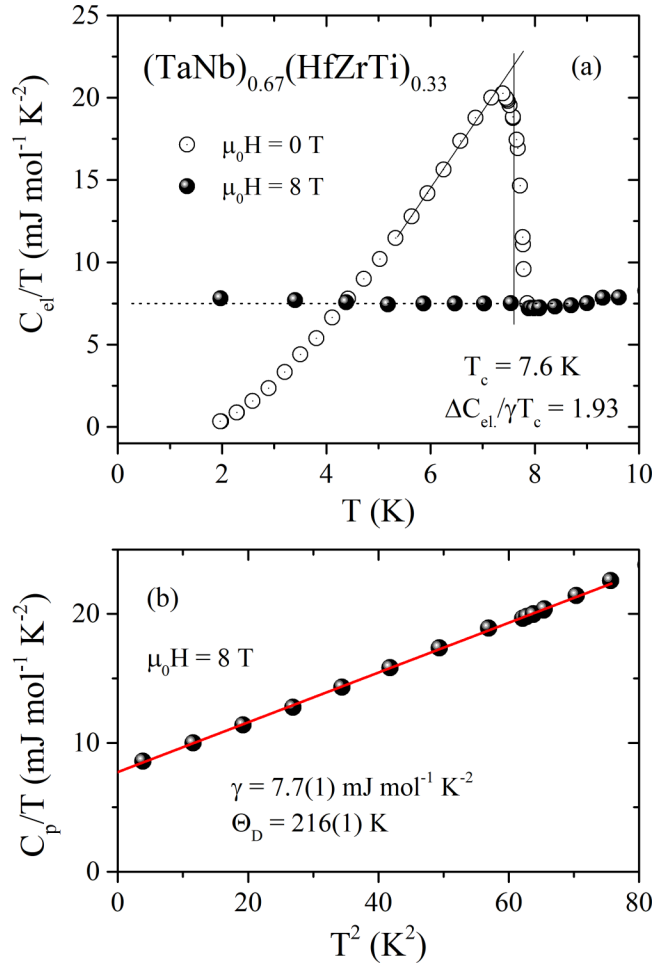

FIG. 5. (a) Temperature dependence of the electronic heat capacity C_{el}/T in zero (open circles) and 8 T (close circles) magnetic field. (b) Low-temperature experimental data C_p/T vs T^2. The solid red line is a fit by the expression $C_p/T = \gamma + \beta T^2$.

TABLE II. Volume thermal expansion coefficient α_V (K^{-1}), zero-pressure Grüneisen parameter (dimensionless), and the bulk modulus B (GPa) of TNHZT, determined in this work, compared to several refractory HEAs [59,60].

	α_V	γ_G^0	B
TNHZT (this work)	2.07	1.62	177.4
TiZrHfVNb	3.60	1.83	79.0
TiZrVNb	3.34	1.65	84.2
TiZrVNbMo	3.32	2.19	125.0
NbTaMoW	2.67	2.40	162.5
NbHfZrTi	2.30		88.3

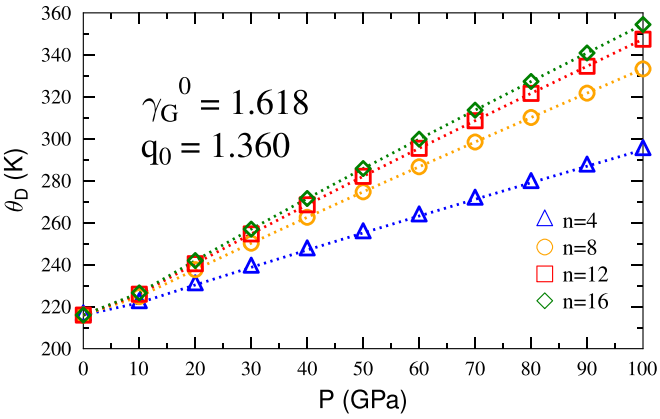

FIG. 6. Simulated pressure dependence of θ_D of TNHZT.

B. Debye temperature under pressure

Evolution of the Debye temperature with pressure, needed to calculate λ in our approach, was simulated according to the model described above. The ambient-pressure Grüneisen parameter γ_G^0 was calculated using Eq. (11). The lattice thermal expansion coefficient and unit-cell volume have been measured experimentally and heat capacity was approximated by the Dulong-Petit law. The parameters $B = 177$ GPa and $B' = 2.87$ were determined from the Birch-Murnaghan equation of state [6]. Values of those parameters are gathered in Table II, along with a data reported for similar alloys [59]. The lattice thermal expansion coefficient of TNHZT is relatively low and it is accompanied by a large bulk modulus. The obtained value of the Grüneisen parameter $\gamma_G^0 = 1.62$ is similar to that found for the other listed alloys. Using Eq. (15), the second-order Grüneisen parameter $q_0 = 1.36$ is obtained. It is larger than q_0 of Nb and Ta, which is a direct consequence of smaller B' observed in TNHZT. Unfortunately, there are no other reported values of q_0 (to the best of our knowledge) among HEAs to compare with. The calculated evolution of θ_D under pressure is shown in Fig. 6 for different values of n. For larger n, $\theta_D(P)$ becomes insensitive to choice of n and we assume $n = 16$ in further analysis. It also gave the closest results to the first-principles modeling and quasiharmonic calculations for Nb and Ta, as described above. Finally, θ_D increases almost linearly with pressure and reaches 360 K at $P = 100$ GPa.

C. Electronic structure

Figure 7 presents total and atomic densities of states of TNHZT, calculated under various pressures. In $(TaNb)_{67}(HfZrTi)_{33}$ and at ambient conditions, the Fermi level is located in the DOS peak, similarly to the first superconducting HEA $Ta_{34}Nb_{33}Hf_8Zr_{14}Ti_{11}$ [10]. Main contributions to the total DOS originate from the d shells of all constituent atoms ($3d$ for Ti, $4d$ for Zr and Nb, and $5d$ for Hf

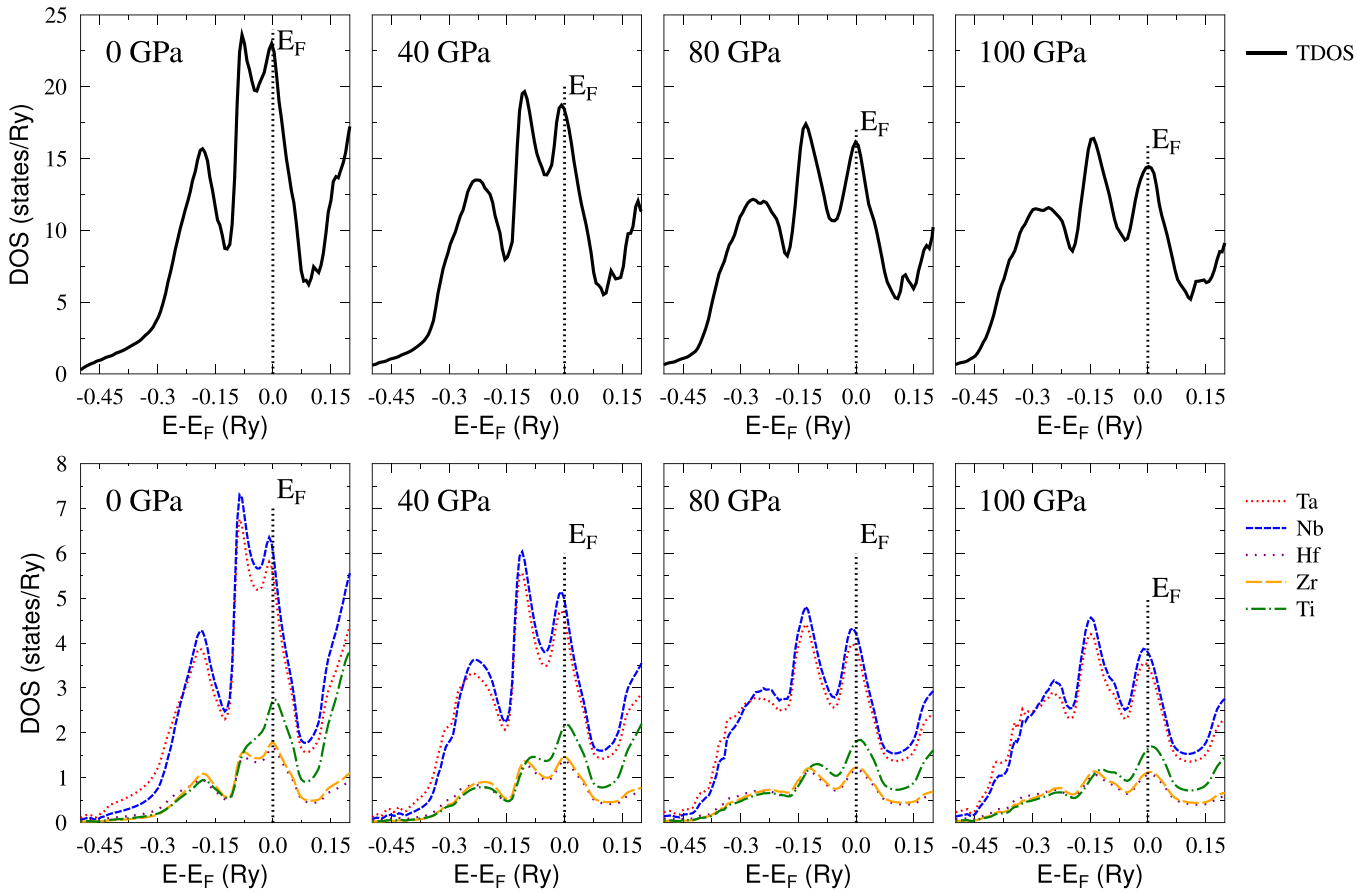

FIG. 7. Total and atomic densities of states of TNHZT alloy, calculated under various pressures in the range of 0 to 100 GPa. Solid black line represents the total DOS. Atomic densities of states are plotted with colors and weighted over its concentrations.

TABLE III. Electronic properties of $(TaNb)_{67}(HfZrTi)_{33}$. M_i is given in u, c_i in %, $N(E_F)$ in Ry^{-1}, η in mRy/a_B^2.

	c_i	M_i	$N(E_F)$	η_i	η_{sp}	η_{pd}	η_{df}
Ta	33.5	181	16.54	151.79	0.83	49.08	101.90
Nb	33.5	93	18.10	157.09	4.46	53.19	99.45
Hf	11	179	15.20	156.30	1.58	66.16	88.60
Zr	11	91	16.21	165.01	6.55	73.16	85.28
Ti	11	41	24.78	119.17	4.80	43.56	70.80

and Ta). As the pressure increases, DOS strongly decreases. It is mainly due to enhanced hybridization and decrease of the unit-cell volume. Furthermore, applied pressure increases separation of the two highest DOS peaks (one located at the Fermi level and the second one below E_F) and shifts electronic states to a lower energy range (i.e., increases the bandwidth). In addition, a shift of electronic states causes a gradual decrease of the third DOS maximum, lying in the lowest-energy range. The atom with the largest contribution to the total DOS at E_F is Ti (see also Table III) for both ambient and elevated pressure conditions. Figure 8 shows the gradual decrease of the $N(E_F)$ value with pressure, from about 22.5 Ry^{-1} to 14.5 Ry^{-1} at 100 GPa. The ambient-pressure value corresponds to the noninteracting Sommerfeld parameter $\gamma_0 = 3.9$ mJ mol^{-1} K^{-2}. Comparison to the experimental value of $\gamma = 7.7(1)$ mJ mol^{-1} K^{-2} gives the electron-phonon enhancement parameter $\lambda = \gamma/\gamma_0 - 1 = 0.97$, which is very close to the value obtained for $Ta_{34}Nb_{33}Hf_8Zr_{14}Ti_{11}$ [10].

In the $N(E_F)$ versus P relation (Fig. 8) we can distinguish three regions. At first, $N(E_F)$ quickly decreases with a slope of -0.123 Ry^{-1}/GPa up to 40 GPa. Above 40 GPa, the decrease becomes slower (-0.042 Ry^{-1}/GPa) and, then, above 70 GPa, the slope becomes more negative, reaching -0.079 Ry^{-1}/GPa. Interestingly, this evolution is correlated with the observed modifications of T_c under pressure, where T_c increases monotonically up to 10 K at around 50 GPa. Above that pressure, the transition temperature remains practically constant. To analyze this trend of $N(E_F)$, electronic dispersion relations were computed using the complex energy band technique, attainable in the KKR-CPA formalism [61–63]. In this

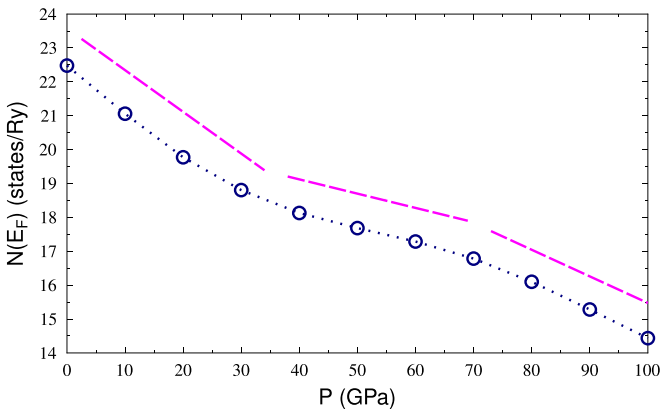

FIG. 8. Variation of the density of states at the Fermi level under hydrostatic pressure from 0 to 100 GPa. Dashed lines are the linear trend lines, described in the text.

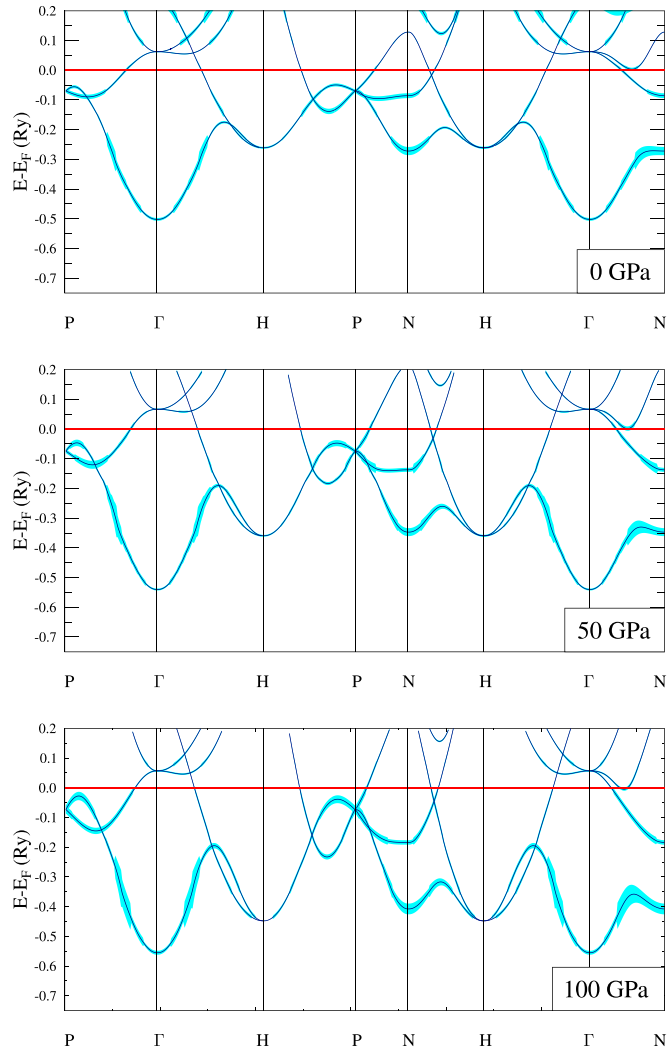

FIG. 9. Electronic dispersion relations for $P = 0$, 50, and 100 GPa. Shading describes the band smearing and corresponds to the imaginary part of the complex energy.

method, the real part of electron energy shows the band center, whereas the imaginary part describes the band smearing effects caused by a chemical disorder. A bandwidth is related to the electronic lifetime that is finite due to the presence of the disorder-induced electron scattering $\tau = \hbar/2\mathrm{Im}(E)$. As we have shown in Ref. [10] in the case of $Ta_{34}Nb_{33}Hf_8Zr_{14}Ti_{11}$, electronic bands were rather sharp with small smearing effect, in spite of the high level of disorder. As seen in Fig. 9 the same situation is found here, especially near E_F, where the small imaginary part of energy gives $\tau \sim 0.5$–1×10^{-14} s. Also, the smearing near E_F does not change much under pressure, although it increases for the lower-lying states.

On the whole, upon external pressure both empty and occupied electronic bands move toward E_F. Interesting evolution is found in the N-Γ direction, where the local minimum of one of the bands is near E_F (peak in DOS is associated with this band). As shown in Fig. 10, above 50 GPa this band comes very close to E_F and its center actually crosses E_F at around ∼70 GPa, leading to a Lifshitz transition [64] (change of the Fermi surface topology). This topological transition is also

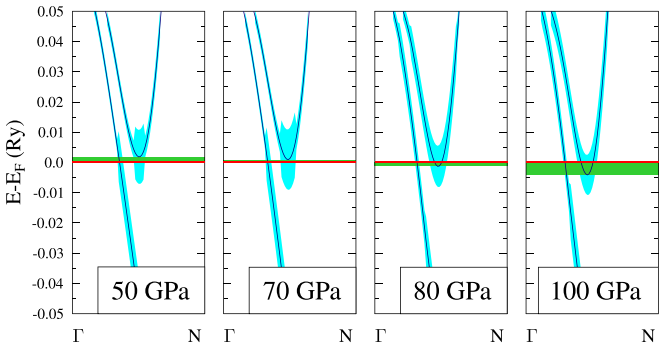

FIG. 10. Electronic dispersion relations near E_F in Γ-N direction, showing the Lifshitz transition. The distance between the center of the band and the Fermi level is marked in green. Shading describes the band smearing and corresponds to the imaginary part of the complex band energy.

visualized in Fig. 11, where k_x-k_y cross sections of the Fermi surface are plotted for 50 and 100 GPa. The appearance of an additional band at the Fermi level is correlated with the slowing down of the decrease in $N(E_F)$ around 40 GPa, as discussed above. The fact that the band is actually blurred by the disorder leads to smearing of this transition and the band starts to contribute to DOS at lower pressures.

What is worth noting, two transitions in topology of electronic states under pressure were reported theoretically [65] for pure Nb: one slight change in the Fermi surface shape at 5–6 GPa and more prominent one around 60 GPa, connected to similar shift in electronic band in N-Γ. In an earlier experiment [66], T_c of Nb was reported to show anomalies around these pressures (increase by 0.7 K and decrease by 1 K, respectively) and changes in the topology of the Fermi surfaces were given as an explanation for these anomalies in Ref. [65]. However, in another theoretical work [67], where relativistic full potential linear muffin-tin orbital (LMTO) calculations were presented, only the second transition was observed, at around 60 GPa of hydrostatic pressure. The first anomaly in T_c, reported in Ref. [66], was ascribed to the presence of nonuniform pressure conditions or polycrystalline sample effects. In our case, the T_c increases monotonically up to about 50 GPa and remains practically constant above that pressure. This trend may be correlated to the observed Lifshitz transition, which is additionally smeared by the disorder effects.

D. Electron-phonon coupling

Values of the ambient-pressure McMillan-Hopfield parameters are gathered in Table III. Titanium, despite its highest $N(E_F)$, has the lowest contribution to the electronic part of the

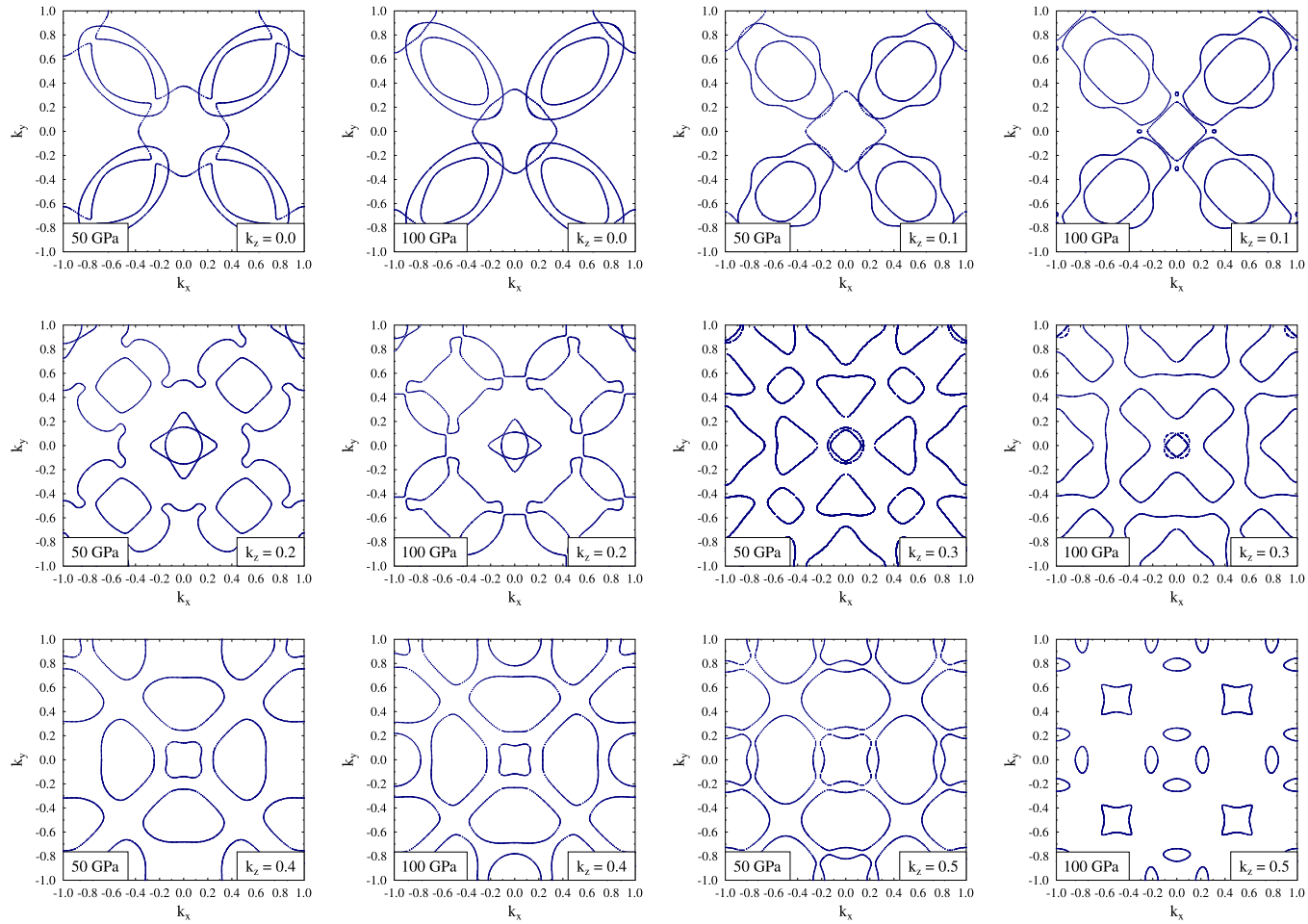

FIG. 11. Cross sections of Fermi surface, calculated under pressures of 50 and 100 GPa. k is given in $2\pi/a$.

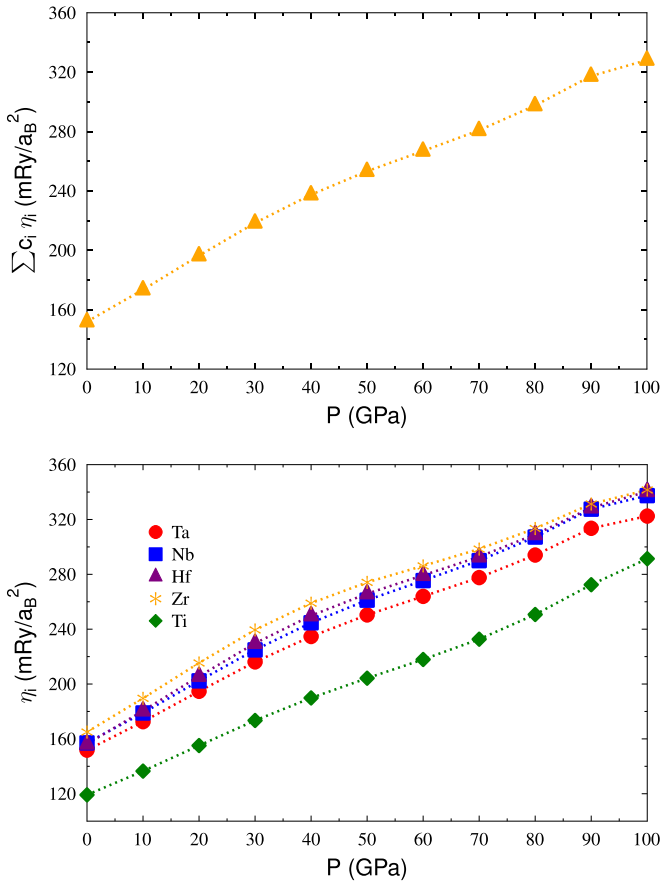

FIG. 12. Pressure evolution of the McMillan-Hopfield parameters: concentration-weighted sum (top) and η_i per atom (bottom).

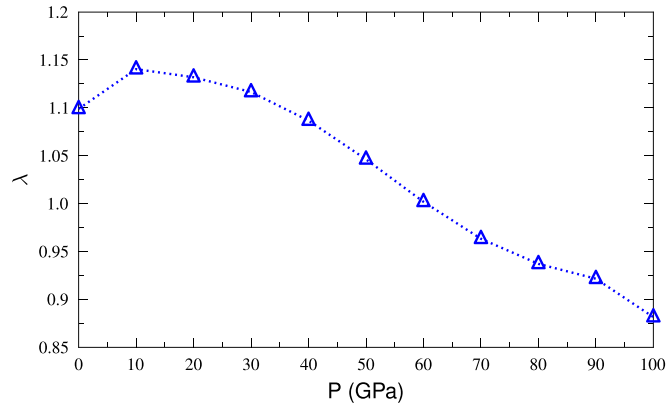

FIG. 14. Calculated evolution of the electron-phonon coupling parameter λ with pressure.

EPC, while the highest belongs to zirconium. Interestingly, Zr atoms also present almost equal contribution to η from the p-d and d-f scattering channels. For other constituent atoms, d-f scattering channel gives the largest contribution to η and it is typical for transition metal elements. To have a reference point, η for pure Nb is about 165 mRy/a$_B^2$ [35], and calculated η_i are slightly smaller than for $Ta_{34}Nb_{33}Hf_8Zr_{14}Ti_{11}$ [10]. Using Eq. (3), the calculated η_i and the experimental Debye temperature $\theta_D = 216$ K, we get the ambient-pressure electron-phonon coupling constant $\lambda = 1.1$. This value is in close agreement with 0.97 determined above from the renormalization of the Sommerfeld coefficient γ.

Evolution of the McMillan-Hopfield parameters with pressure is shown in Fig. 12: a concentration-weighted sum in the top panel and η_i per atom in the bottom panel. In both cases, the evolution is very smooth, with gradual increase in η. What can be noticed in Fig. 12 is the slight change of slope of the curve, above 40–50 GPa, which resembles the one seen in $N(E_F)$ variation in Fig. 8. Nevertheless, the evolution of η is rather typical, as η generally increases with pressure [29,68,69]. Less obvious is the change of the distribution of η among the s-p-d-f scattering channels, which is plotted in Fig. 13. For the group 4 elements, i.e., Hf, Zr, Ti, a change of the dominating scattering channel to p-d at high pressures is observed. Such a behavior is not observed for Ta and Nb atoms, although values of η_{pd} and η_{df} become close to each other. The increase in η_i is related to the increase in the matrix elements in Eq. (2), which we additionally plotted in the Supplemental Material [34].

The pressure evolution of λ, obtained based on computed $\eta_i(P)$ parameters (Fig. 12), simulated evolution of Debye temperature $\theta_D(P)$ (Fig. 6), and Eq. (3) is shown in Fig. 14. After an initial increase, we observe a general decrease in λ. This is due to the fact that the evolution of the electron-phonon coupling constant λ with pressure is the result of two competitive effects: an increase of the McMillan-Hopfield η

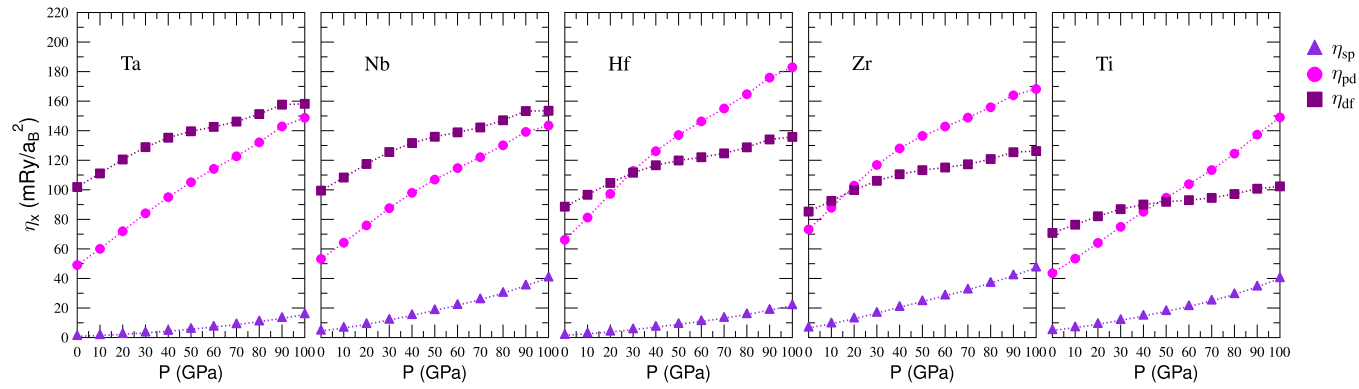

FIG. 13. Evolution of the McMillan-Hopfield parameters of each of the atoms, decomposed over the $l \rightarrow l+1$ scattering channels.

and increase of the phonon frequencies ω, here represented by the Debye temperature θ_D. Taking the derivative of $\ln\lambda$ from Eq. (3) we get

$$\frac{d\ln\lambda}{dP} = -\frac{1}{\tilde{B}}\left(\frac{d\ln\eta}{d\ln V} + 2\gamma_G\right), \tag{18}$$

where $\eta = \sum_i c_i\eta_i$ and $\gamma_G = -\frac{d\ln\theta_D}{d\ln V}$. The simplified pressure-volume equation of state $V = V_0\exp(-P/\tilde{B})$ was used to convert the pressure derivative into the volume one. The value of such-defined $\tilde{B}$ "bulk modulus" is of no importance here for the qualitative discussion. The McMillan-Hopfield parameters increase when the unit-cell volume decreases, thus, $\frac{d\ln\eta}{d\ln V}$ is negative [29,68,69] and its value is usually between -1.0 and -3.0. From the equation above, we can see that $\lambda(P)$ would be an increasing function of pressure for the case where $-\frac{d\ln\eta}{d\ln V} > 2\gamma_G$. In our case, $2\gamma_G \simeq 3.0$ and $-\frac{d\ln\eta}{d\ln V} < 3.0$ for all pressures above 20 GPa, and, therefore, a decreasing $\lambda(P)$ function is expected. This is exactly what we can see in Fig. 14, where λ decreases with pressure above 10 GPa. Only at 10 GPa, due to the strong increase of η, an increase of calculated λ is observed since the condition $-\frac{d\ln\eta}{d\ln V} > 2\gamma_G$ is fulfilled. At ambient conditions we have $\lambda = 1.10$. It raises to $\lambda \simeq 1.15$ at 10 GPa and then gradually decreases for larger pressures, reaching 0.88 at 100 GPa.

Finally, the superconducting critical temperature may be calculated using the McMillan formula [32]

$$T_c = \frac{\theta_D}{1.45}\exp\left[-\frac{1.04(1+\lambda)}{\lambda - \mu^*(1+0.62\lambda)}\right]. \tag{19}$$

The last parameter which has to be determined is the Coulomb pseudopotential parameter μ^*. In zero pressure, the most commonly used value of 0.13 would lead to an overestimated $T_c = 12.5$ K. To get the experimental zero pressure $T_c = 7.7$ K one has to use $\mu^* = 0.215$. Similar value was used for pure Nb to reproduce the experimental critical temperature based on the calculated Eliashberg function [67,70]. Even larger values of μ^* were postulated for other materials such as Nb_3Ge ($\mu^* = 0.24$) [71], V ($\mu^* = 0.3$) [70], or $MgCNi_3$ ($\mu^* = 0.29$) [72]. Thus, to explore the variation of T_c with pressure, we assume $\mu^*(0) = 0.215$. For $P > 0$, $T_c(P)$ was calculated in two ways. First, $\mu^* = 0.215$ was kept constant in the whole pressure range. Next, $\mu^*(P)$ dependence was assumed to originate from the pressure dependence of $N(E_F)$ and calculated using the Benneman and Garland formula [73]

$$\mu^* = \frac{AN(E_F)}{1+N(E_F)}, \tag{20}$$

where $N(E_F)$ is in eV^{-1} per atom. Originally, Benneman and Garland set $A = 0.26$ to get $\mu^* = 0.13$ for the typical case of a metal with $N(E_F) = 1$ eV^{-1} per atom. Therefore, in our case where $N(E_F) = 1.65$ eV^{-1} for $P = 0$ and postulated $\mu^*(0) = 0.215$ we use $A = 0.345$, and simulate $\mu^*(P)$ dependence according to $N(E_F)$ variation with pressure (Fig. 8) by using Eq. (20). Figure 15 shows the $\mu^*(P)$ dependence that decreases smoothly with pressure and drops to 0.17 at 100 GPa. Finally, Fig. 16 shows the computed critical temperature $T_c(P)$, where T_c for the "standard" $\mu^* = 0.13$ as also included.

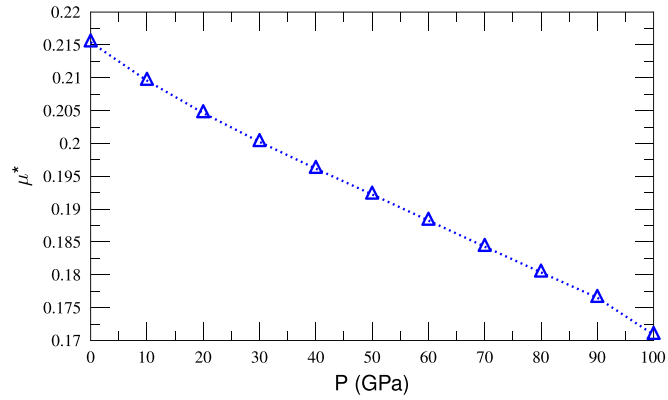

FIG. 15. Variation of the Coulomb pseudopotential parameter μ^* with pressure, calculated using Eq. (20) and $N(E_F)$ as in Fig. 8.

In general, under the assumption of relatively large $\mu^*(0) = 0.215$, our calculations quite well predict the variation of T_c with pressure [but only when variable $\mu^*(P)$ is used]. In spite of the decrease in the computed λ above 10 GPa, T_c increases up to 40–50 GPa and then remains almost constant up to 100 GPa, just like it is observed in the experiment. This counterintuitive observation shows the delicate balance between T_c, θ_D, and λ since an increase in θ_D leads to a quadratic increase in the denominator of Eq. (3) (tendency to decrease λ) and linear increase of T_c via the multiplicator in McMillan's Eq. (19). In stabilization of T_c above 40 GPa, the decrease of μ^*, which results from the decrease in $N(E_F)$, occurs to be equally important since for the constant μ^* decrease in T_c is predicted by the theoretical calculations. This shows that up to a studied pressure of 100 GPa, the evolution of T_c with pressure in $(TaNb)_{0.67}(HfZrTi)_{0.33}$ can be explained by the classical electron-phonon mechanism. This is surprisingly well captured by a combination of coherent potential approximation, rigid muffin-tin approximation, and "averaged" phonon spectrum. Thus, structural local short-range ordering effects or local distortions of the crystal structure that are likely present in the studied samples, seem not

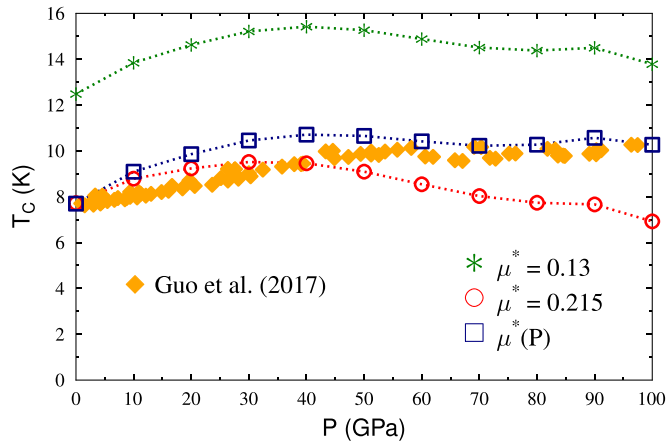

FIG. 16. Calculated pressure dependence of T_c of $(TaNb)_{0.67}(HfZrTi)_{0.33}$ for two constant values of $\mu^* = 0.13$ and 0.215, variable $\mu^*(P)$ (see Fig. 15), and compared to experiment [6].

to have a large impact on superconductivity. This may be understood as the superconducting coherence length being typically much larger than the structural anomalies' length scale. Based on the upper critical field data from Ref. [15] ($\mu_0 H_{c2} = 7.75$ T) the superconducting coherence length may be estimated as 65 Å. This is is roughly 20 times the lattice parameter of the system. On this length scale, the possible local crystal structure distortions or chemical inhomogeneities are averaged out, and therefore an effective medium theory that we apply here, works well.

IV. SUMMARY

In summary, we have studied pressure effects of the electronic structure, electron-phonon interaction, and superconductivity of the high entropy alloy $(TaNb)_{0.67}(HfZrTi)_{0.33}$ in a pressure range from 0 to 100 GPa. With increasing pressure, the total density of states at the Fermi level $N(E_F)$ gradually decreases. Lifshitz transition is observed around 70 GPa when one of the bands starts crossing the Fermi level. Due to disorder-induced band smearing effects, however, the transition is not sharp since these bands contribute to $N(E_F)$ also at lower pressures (even below 50 GPa). As in the experimental studies, $T_c(P)$ changes the slope above 50 GPa and this effect may be correlated with the calculated band-structure evolution and the Lifshitz transition. The effects of pressure on the lattice dynamics were simulated using the Debye-Grüneisen model, where γ_G parameter was additionally determined. The calculated McMillan-Hopfield parameters increase with pressure, but due to concurrent effect of the lattice stiffening and increase of the Debye temperature, the electron-phonon coupling parameter λ decreases above 10 GPa. In spite of this, the calculated superconducting T_c increases up to 40–50 GPa and later is stabilized at the larger value of λ than observed at the ambient conditions. This nondecreasing T_c results from the increase of the Debye temperature and decrease of $N(E_F)$, which is caused by the monotonic decrease of the Coulomb pseudopotential parameter μ^*. Our results are in good agreement with the experimental trend and show that up to a studied pressure of 100 GPa, the evolution of T_c with pressure in $(TaNb)_{0.67}(HfZrTi)_{0.33}$ can be well explained by the classical electron-phonon mechanism. This implies that the electronic structure of the system is well described by the coherent potential approximation. An excellent additional test of our theoretical results would be a measurement of the electronic heat capacity under pressure, which would allow verification of the observed decrease in both $N(E_F)$ and λ.

ACKNOWLEDGMENTS

K.J. and B.W. were supported by the National Science Center (Poland), Grant No. 2017/26/E/ST3/00119. K. Gofryk acknowledges support from DOE's Early Career Research Program. J.T. was supported by the AGH-UST statutory tasks No. 11.11.220.01/5 within subsidy of the Ministry of Science and Higher Education.

[1] A. P. Drozdov, M. I. Eremets, I. A. Troyan, V. Ksenofontov, and S. I. Shylin, Conventional superconductivity at 203 kelvin at high pressures in the sulfur hydride system, Nature (London) **525**, 73 (2015).

[2] A. P. Drozdov, P. P. Kong, V. S. Minkov, S. P. Besedin, M. A. Kuzovnikov, S. Mozaffari, L. Balicas, F. F. Balakirev, D. E. Graf, V. B. Prakapenka, E. Greenberg, D. A. Knyazev, M. Tkacz, and M. I. Eremets, Superconductivity at 250 K in lanthanum hydride under high pressures, Nature (London) **569**, 528 (2019).

[3] R. Szczęśniak and A. P. Durajski, Superconductivity well above room temperature in compressed MgH_6, Front. Phys. **11**, 117406 (2016).

[4] R. Szczęśniak and A. P. Durajski, Unusual sulfur isotope effect and extremely high critical temperature in H_3S superconductor, Sci. Rep. **8**, 6037 (2018).

[5] J. Guo, G. Lin, S. Cai, C. Xi, C. Zhang, W. Sun, Q. Wang, K. Yang, A. Li, Q. Wu, Y. Zhang, T. Xiang, R. J. Cava, and L. Sun, Record-high superconductivity in Niobium-Titanium alloy, Adv. Mater. **31**, 1807240 (2019).

[6] J. Guo, H. Wang, F. von Rohr, Z. Wang, S. Cai, Y. Zhou, K. Yang, A. Li, S. Jiang, Q. Wu, R. J. Cava, and L. Sun, Robust zero resistance in a superconducting high-entropy alloy at pressures up to 190 GPa, Proc. Natl. Acad. Sci. USA **114**, 13144 (2017).

[7] J.-W. Yeh, S.-K. Chen, S.-J. Lin, J.-Y. Gan, T.-S. Chin, T.-T. Shun, C.-H. Tsau, and S.-Y. Chang, Nanostructured high-entropy alloys with multiple principal elements: Novel alloy design concepts and outcomes, Adv. Eng. Mater. **6**, 299 (2004).

[8] J. W. Yeh, Y. L. Chen, S. J. Lin, and S. K. Chen, High-entropy alloys-A new era of exploitation, in *Advanced Structural Materials III*, Materials Science Forum, Vol. 560 (Trans Tech Publications, Switzerland, 2007), pp. 1.

[9] P. Koželj, S. Vrtnik, A. Jelen, S. Jazbec, Z. Jagličić, S. Maiti, M. Feuerbacher, W. Steurer, and J. Dolinšek, Discovery of a Superconducting High-Entropy Alloy, Phys. Rev. Lett. **113**, 107001 (2014).

[10] K. Jasiewicz, B. Wiendlocha, P. Korbeń, S. Kaprzyk, and J. Tobola, Superconductivity of $Ta_{34}Nb_{33}Hf_8Zr_{14}Ti_{11}$ high entropy alloy from first principles calculations, Phys. Status Solidi: Rapid Res. Lett. **10**, 415 (2016).

[11] R. Sogabe, Y. Goto, and Y. Mizuguchi, Superconductivity in $REO_{0.5}F_{0.5}BiS_2$ with high-entropy-alloy-type blocking layers, Appl. Phys. Express **11**, 053102 (2018).

[12] K. Stolze, J. Tao, F. O. von Rohr, T. Kong, and R. J. Cava, Sc-Zr-Nb-Rh-Pd and Sc-Zr-Nb-Ta-Rh-Pd high-entropy alloy superconductors on a CsCl-type lattice, Chem. Mater. **30**, 906 (2018).

[13] K. Stolze, F. A. Cevallos, T. Kong, and R. J. Cava, High-entropy alloy superconductors on an σ-Mn lattice, J. Mater. Chem. C **6**, 10441 (2018).

[14] F. O. von Rohr and R. J. Cava, Isoelectronic substitutions and aluminium alloying in the Ta-Nb-Hf-Zr-Ti high-entropy alloy superconductor, Phys. Rev. Mater. **2**, 034801 (2018).

[15] F. von Rohr, M. J. Winiarski, J. Tao, T. Klimczuk, and R. J. Cava, Effect of electron count and chemical complexity in the Ta-Nb-Hf-Zr-Ti high-entropy alloy superconductor, Proc. Natl. Acad. Sci. USA **113**, E7144 (2016).

[16] T. Stopa, S. Kaprzyk, and J. Tobola, Linear aspects of the Korringa–Kohn–Rostoker formalism, J. Phys.: Condens. Matter **16**, 4921 (2004).

[17] S. Kaprzyk and A. Bansil, Green's function and a generalized lloyd formula for the density of states in disordered muffin-tin alloys, Phys. Rev. B **42**, 7358 (1990).

[18] A. Bansil, S. Kaprzyk, P. E. Mijnarends, and J. Toboła, Electronic structure and magnetism of $Fe_{3-x}V_xX (X = Si, Ga, and Al)$ alloys by the KKR-CPA method, Phys. Rev. B **60**, 13396 (1999).

[19] P. Soven, Coherent-potential model of substitutional disordered alloys, Phys. Rev. **156**, 809 (1967).

[20] G. D. Gaspari and B. L. Gyorffy, Electron-Phonon Interactions, *d* Resonances, and Superconductivity in Transition Metals, Phys. Rev. Lett. **28**, 801 (1972).

[21] J. P. Perdew and Y. Wang, Accurate and simple analytic representation of the electron-gas correlation energy, Phys. Rev. B **45**, 13244 (1992).

[22] K. Jasiewicz, J. Cieslak, S. Kaprzyk, and J. Tobola, Relative crystal stability of Al_xFeNiCrCo high entropy alloys from XRD analysis and formation energy calculation, J. Alloys Compd. **648**, 307 (2015).

[23] K. Jin, B. C. Sales, G. M. Stocks, G. D. Samolyuk, M. Daene, W. J. Weber, Y. Zhang, and H. Bei, Tailoring the physical properties of ni-based single-phase equiatomic alloys by modifying the chemical complexity, Sci. Rep. **6**, 20159 (2016).

[24] M. Calvo-Dahlborg, J. Cornide, J. Tobola, D. Nguyen-Manh, J. S. Wróbel, J. Juraszek, S. Jouen, and U. Dahlborg, Interplay of electronic, structural and magnetic properties as the driving feature of high-entropy CoCrFeNiPd alloys, J. Phys. D: Appl. Phys. **50**, 185002 (2017).

[25] K. Jasiewicz, S. Kaprzyk, and J. Tobola, Interplay of Crystal Structure Preference and Magnetic Ordering in High Entropy CrCoFeNiAl Alloys, Acta Phys. Pol. A **133**, 511 (2018).

[26] I. R. Gomersall and B. L. Gyorffy, A simple theory of the electron-phonon mass enhancement in transition metal compounds, J. Phys. F: Met. Phys. **4**, 1204 (1974).

[27] B. M. Klein, L. L. Boyer, and D. A. Papaconstantopoulos, Superconducting Properties of *A*15 Compounds Derived from Band-Structure Results, Phys. Rev. Lett. **42**, 530 (1979).

[28] I. I. Mazin, S. N. Rashkeev, and S. Y. Savrasov, Nonspherical rigid-muffin-tin calculations of electron-phonon coupling in high-T_c perovskites, Phys. Rev. B **42**, 366 (1990).

[29] B. Wiendlocha, J. Tobola, and S. Kaprzyk, Search for Sc_3XB$(X = In, Tl, Ga, Al)$ perovskites superconductors and proximity of weak ferromagnetism, Phys. Rev. B **73**, 134522 (2006).

[30] B. Wiendlocha, J. Tobola, M. Sternik, S. Kaprzyk, K. Parlinski, and A. M. Oleś, Superconductivity of Mo_3Sb_7 from first principles, Phys. Rev. B **78**, 060507(R) (2008).

[31] B. Wiendlocha and M. Sternik, Effect of the tetragonal distortion on the electronic structure, phonons and superconductivity in the Mo_3Sb_7 superconductor, Intermetallics **53**, 150 (2014).

[32] W. L. McMillan, Transition temperature of strong-coupled superconductors, Phys. Rev. **167**, 331 (1968).

[33] J. J. Hopfield, Angular momentum and transition-metal superconductivity, Phys. Rev. **186**, 443 (1969).

[34] See Supplemental Material at http://link.aps.org/supplemental/10.1103/PhysRevB.100.184503 for the discussion of the different definitions of the frequency moments, Figs. S1 and S2, for the phonon DOS plots of Nb and Ta under pressure, Fig. S3 for the XRD pattern at room temperature, and Fig. S4 for the plot of the matrix elements, which enter the formula for the McMillan-Hopfield parameters.

[35] S. S. Rajput, R. Prasad, R. M. Singru, S. Kaprzyk, and A. Bansil, Electronic structure of disordered Nb - Mo alloys studied using the charge-self-consistent Korringa - Kohn - Rostoker coherent potential approximation, J. Phys.: Condens. Matter **8**, 2929 (1996).

[36] D. A. Papaconstantopoulos, L. L. Boyer, B. M. Klein, A. R. Williams, V. L. Morruzzi, and J. F. Janak, Calculations of the superconducting properties of 32 metals with $Z \leqslant 49$, Phys. Rev. B **15**, 4221 (1977).

[37] S. Massidda, J. Yu, and A. J. Freeman, Electronic structure and properties of superconducting $LiTi_2O_4$, Phys. Rev. B **38**, 11352 (1988).

[38] F. Birch, Finite elastic strain of cubic crystals, Phys. Rev. **71**, 809 (1947).

[39] Z.-L. Liu, L.-C. Cai, X.-R. Chen, Q. Wu, and F.-Q. Jing, *Ab initio* refinement of the thermal equation of state for bcc tantalum: The effect of bonding on anharmonicity, J. Phys.: Condens. Matter **21**, 095408 (2009).

[40] G. Grimvall, *Thermophysical Properties of Materials* (North-Holland, Amsterdam, 1986).

[41] R. Jeanloz, Shock wave equation of state and finite strain theory, J. Geophys. Res.: Solid Earth **94**, 5873 (1989).

[42] C. Nie, Volume and temperature dependence of the second Grüneisen parameter of NaCl, Phys. Status Solidi B **219**, 241 (2000).

[43] O. L. Anderson and D. G. Isaak, The dependence of the Anderson-Grüneisen parameter δ_T upon compression at extreme conditions, J. Phys. Chem. Solids **54**, 221 (1993).

[44] O. L. Anderson, *Equations of State for Solids in Geophysics and Ceramic Science* (Oxford University Press, New York, 1995).

[45] O. L. Anderson, Derivation of Wachtman's equation for the temperature dependence of elastic moduli of oxide compounds, Phys. Rev. **144**, 553 (1966).

[46] J. S. Dugdale and D. K. C. MacDonald, The thermal expansion of solids, Phys. Rev. **89**, 832 (1953).

[47] Y. A. Chang, On the temperature dependence of the bulk modulus and the Anderson-Grüneisen parameter δ of oxide compounds, J. Phys. Chem. Solids **28**, 697 (1967).

[48] Y. Kimura, T. Ohtsuka, T. Matsui, and T. Mizusaki, The normal state specific heat of niobium-tantalum alloys, Phys. Lett. A **29**, 284 (1969).

[49] A. F. Guillermet and G. Grimvall, Homology of interatomic forces and debye temperatures in transition metals, Phys. Rev. B **40**, 1521 (1989).

[50] I. S. Grigoriev and E. Z. Meilikhov, *Handbook of Physical Quantities* (CRC Press, New York, 1997).

[51] K. W. Katahara, M. H. Manghnani, and E. S. Fisher, Pressure derivatives of the elastic moduli of BCC Ti-V-Cr, Nb-Mo and Ta-W alloys, J. Phys. F: Met. Phys. **9**, 773 (1979).

[52] K. A. Jr Gschneidner, *Solid State Physics* (Academic, New York, 1964).

[53] P. Giannozzi, S. Baroni, N. Bonini, M. Calandra, R. Car, C. Cavazzoni, D. Ceresoli, G. L. Chiarotti, M. Cococcioni, I. Dabo, A. Dal Corso, S. de Gironcoli, S. Fabris, G. Fratesi, R. Gebauer, U. Gerstmann, C. Gougoussis, A. Kokalj, M. Lazzeri, L. Martin-Samos *et al.*, QUANTUM ESPRESSO: A modular and open-source software project for quantum simulations of materials, J. Phys.: Condens. Matter **21**, 395502 (2009).

[54] P. Giannozzi, O. Andreussi, T. Brumme, O. Bunau, M. B. Nardelli, M. Calandra, R. Car, C. Cavazzoni, D. Ceresoli, M. Cococcioni, N. Colonna, I. Carnimeo, A. D. Corso, S. de Gironcoli, P. Delugas, R. A. DiStasio Jr, A. Ferretti, A. Floris, G. Fratesi, G. Fugallo *et al.*, Advanced capabilities for materials modeling with QUANTUM ESPRESSO, J. Phys.: Condens. Matter **29**, 465901 (2017).

[55] A. D. Corso, Pseudopotentials periodic table: From H to Pu, Comput. Mater. Sci. **95**, 337 (2014).

[56] The following pseudopotentials were used: Ta.pbe-spfn-kjpaw_psl.1.0.0.UPF and Nb.pbe-spn-kjpaw_psl.1.0.0.UPF, http://www.quantum-espresso.org/pseudopotentials/

[57] J. P. Perdew, K. Burke, and M. Ernzerhof, Generalized Gradient Approximation Made Simple, Phys. Rev. Lett. **77**, 3865 (1996).

[58] G. Grimvall, *The Electron-phonon Interaction in Metals* (North-Holland, Amsterdam, 1981).

[59] X. Li, First-principles study of the third-order elastic constants and related anharmonic properties in refractory high-entropy alloys, Acta Mater. **142**, 29 (2018).

[60] A. S. Ahmad, Y. Su, S. Y. Liu, K. Ståhl, Y. D. Wu, X. D. Hui, U. Ruett, O. Gutowski, K. Glazyrin, H. P. Liermann, H. Franz, H. Wang, X. D. Wang, Q. P. Cao, D. X. Zhang, and J. Z. Jiang, Structural stability of high entropy alloys under pressure and temperature, J. Appl. Phys. **121**, 235901 (2017).

[61] A. Bansil, Coherent-potential and average t-matrix approximations for disordered muffin-tin alloys. II. Application to realistic systems, Phys. Rev. B **20**, 4035 (1979).

[62] W. H. Butler, Theory of electronic transport in random alloys: Korringa-Kohn-Rostoker coherent-potential approximation, Phys. Rev. B **31**, 3260 (1985).

[63] B. Wiendlocha, K. Kutorasinski, S. Kaprzyk, and J. Tobola, Recent progress in calculations of electronic and transport properties of disordered thermoelectric materials, Scr. Mater. **111**, 33 (2016).

[64] I. M. Lifshitz, Anomalies of electron characteristics of a metal in the high pressure region, ZhETF, **38**, 1569, (1960) [J. Exp. Theor. Phys. **11**, 1130 (1960)].

[65] J. S. Tse, Z. Li, K. Uehara, Y. Ma, and R. Ahuja, Electron-phonon coupling in high-pressure Nb, Phys. Rev. B **69**, 132101 (2004).

[66] V. V. Struzhkin, Y. A. Timofeev, R. J. Hemley, and H.-K. Mao, Superconducting T_c and Electron-Phonon Coupling in Nb to 132 GPa: Magnetic Susceptibility at Megabar Pressures, Phys. Rev. Lett. **79**, 4262 (1997).

[67] S. A. Ostanin, V. Yu. Trubitsin, S. Yu. Savrasov, M. Alouani, and H. Dreyssé, Calculated Nb superconducting transition temperature under hydrostatic pressure, High Press. Res. **17**, 393 (2000).

[68] V. K. Ratti, R. Evans, and B. L. Gyorffy, The volume dependence of the electron-phonon mass enhancement and the pressure dependence of tc in transition metals, J. Phys. F: Met. Phys. **4**, 371 (1974).

[69] B. Wiendlocha, M. J. Winiarski, M. Muras, C. Zvoriste-Walters, J.-C. Griveau, S. Heathman, M. Gazda, and T. Klimczuk, Pressure effects on the superconductivity of the $HfPd_2Al$ Heusler compound: Experimental and theoretical study, Phys. Rev. B **91**, 024509 (2015).

[70] S. Y. Savrasov and D. Y. Savrasov, Electron-phonon interactions and related physical properties of metals from linear-response theory, Phys. Rev. B **54**, 16487 (1996).

[71] J. P. Carbotte, Properties of boson-exchange superconductors, Rev. Mod. Phys. **62**, 1027 (1990).

[72] R. Szczęśniak, A. P. Durajski, and ŁHerok, Thermodynamic properties of antiperovskite $MgCNi_3$ in superconducting phase, Solid State Commun. **203**, 63 (2015).

[73] J. W. Garland and K. H. Bennemann, Theory for the pressure dependence of Tc for narrow-band superconductors, AIP Conf. Proc. **4**, 255 (1972).

Correction: The bottom panel of Fig. 12 and all panels in Fig. 13 contained errors in the presentation of the McMillan-Hopfield parameters and have been replaced.